Springer

KSME

Journal of Mechanical Science and Technology 26 (5) (2012) 1567~1575
www.springerlink.com/content/1738-494x
DOI 10.1007/s12206-012-0327-5

Optimal design of spaced plates under hypervelocity impact †

Younghoon Kim[1], Jeonghoon Yoo[2,*] and Minhyung Lee[3]

[1]*Graduate School of Mechanical Engineering, Yonsei University, Seoul, 120-749, Korea*
[2]*School of Mechanical Engineering, Yonsei University, Seoul, 120-749, Korea*
[3]*School of Mechanical and Aerospace Engineering, Sejong University, Seoul, 143-747, Korea*

(Manuscript Received August 25, 2011; Revised November 28, 2011; Accepted February 9, 2012)

Abstract

This paper presents a bumper shield design for protection of a satellite structure system subjected to hypervelocity impact (above 6 km/s) from space debris. Especially, this study is focused on the optimization of the spaced plates (the so-called Whipple shield) design using the coupled SPH and Lagrangian FEM methods. This is because the SPH is a meshless method and it is efficient in hypervelocity impact analysis involving debris caused by fragmentation and penetration under hypervelocity impact. The Whipple shield is composed of multiple spaced plates where the first bumper plate is modeled as particles for SPH simulation while the rear wall is modeled as elements for FEM. The appropriate smoothing length and mesh size were determined taking into account computational cost and accuracy and the erosion scheme is adopted to avoid numerical error due to large deformation. After verification for the comparison with previous experimental works, the optimal plate structure is proposed considering multi design objectives based on parameter optimization.

Keywords: Hypervelocity impact; Smoothed particle hydrodynamics (SPH); Finite element method (FEM); Parameter optimization; Multi-objective optimization

1. Introduction

Recently, growing interest in space has led to various studies regarding structural behavior for exceptional cases such as the hypervelocity impact. The importance of protecting a spacecraft, a satellite or a guided weapon against hypervelocity debris such as meteors and meteoroids is increasing. When hypervelocity impact occurs, large deformation and fracture are produced by hydrodynamic movement due to the high kinetic energy [1].

The aim of this study is to design the multi-plate structure of a satellite to absorb the kinetic energy generated by hypervelocity debris during the impact. For the purpose, analysis and design are performed in order to prevent the penetration of the final bumper plate of the satellite. A number of previous studies associated with hypervelocity impact have been performed using the numerical method as well as the experimental method [2-5]. Experimental methods generally require expensive equipment and require enormous time and cost. On the contrary, numerical methods need to define appropriate assumptions and simplifications for the phenomenon to guarantee accuracy in spite of their low cost and convenience. The hypervelocity impact analysis using the numerical program is widely performed mostly due to limitation of impact speed in experiments.

The finite element method (FEM) is widely used for the structure problem, while the smoothed particle hydrodynamics (SPH) is mainly used for astrophysics and studies related with the high-deformation problem [8]. In this study, the FEM [2-4] and the SPH [6-8] are combined as a numerical method. Various conditions need to be considered. First, a strength model is selected with its material properties [9]. Also, the proper smoothing length known as the radius of a particle domain must be arranged in the SPH application [10, 11]. For the coupling of the FEM and the SPH, an appropriate contact method must be chosen [12-14]. In case of hypervelocity analysis using FEM, since the excessive element deformation causes numerical error, the erosion scheme to overcome such disadvantage is required [15, 16]. The verification of the simulation result using AUTODYN, which is adopted for the simulation tool in this study, through the comparison with the experiment method is conducted. For this purpose, experimental data based on Piekutowski's works [17, 18] are used.

For the Whipple shield problem, the previous experimental data [19] are simulated as a model case, and then optimization study is conducted to evaluate the existence of a possible better design. For the optimal design, parameter optimization is performed to control the thickness of each plate and the dis-

*Corresponding author. Tel.: +82 2 2123 2859
E-mail address: yoojh@yonsei.ac.kr
† Recommended by Associate Editor Chang-Wan Kim.

tance between plates using the design of experiment (DOE) and the response surface method (RSM) for two cases. Optimal design for dual plates for the multi-objective of minimizing the plastic work and total mass is considered for the first case. Next, total mass of a triple-plate structure is targeted to be minimized satisfying the non-penetration condition of the final rear plate.

2. Hypervelocity impact analysis

2.1 Material models

In the hypervelocity impact considered in this study, the projectile is composed of Al2024-T4 while the bumper and the contact plates are made of Al6061-T6. The simulation is performed using the commercial package AUTODYN based on the Steinberg-Guinan model [9, 16]. The effect of melting on the deviatoric response is included through the use of the thermal softening component in the model. The shear modulus can be represented as

$$G = G_0\left\{1+(\frac{G_P^{'}}{G_0})\frac{p}{\eta^{1/2}}+(\frac{G_T^{'}}{G_0})(T-300)\right\} \quad (1)$$

where G_0 is the reference shear modulus, and T_0 is the reference temperature. $G_P^{'}$ and $G_T^{'}$ are material constants according to pressure and temperature, respectively. P is the pressure, and η is the compression rate as v/v_0. The yield stress is expressed as follows:

$$Y = Y_0\left\{1+(\frac{Y_P^{'}}{Y_0})\frac{p}{\eta^{1/2}}+(\frac{G_T^{'}}{G_0})(T-300)(1+\beta\varepsilon)^n\right\}, \quad (2)$$

and $Y_0(1+\beta\varepsilon)^n \le Y_{\max}$

where Y_0 is the reference yield stress, and $Y_P^{'}$ is a material constants according to the pressure. Y_{max} and ε are the maximum yield stress and the effective plastic strain, respectively. η is the hardening exponent. In Table 1, the material properties regarding the Steinberg-Guinan model for AUTODYN analysis are listed.

Table 1. Material property used in the Steinberg-Guinan model.

Material parameter		Unit	Al 2024-T4 (Projectile)	Al 6061-T6 (Plate)
Density (ρ)		g/mm^3	2.785	2.703
Shear modulus (G)		kpa	2.86×10^7	2.76×10^7
Yield stress (Y)		kpa	2.6×10^5	2.9×10^5
Maximum yield stress (Y_{max})		kpa	7.6×10^5	6.8×10^5
Material constant	Hardening constant (β)	none	310	125
	Hardening exponent (n)	none	0.185	0.100
	Derivative dg/dT ($G_T^{'}$)	kpa/K	-1.762×10^4	-1.70×10^4
	Derivative dg/dp ($G_P^{'}$)	none	1.8647	1.8000
	Derivative dy/dp ($Y_P^{'}$)	none	0.016950	0.018908
	Melting temperature (T)	K	1.22×10^3	1.22×10^3

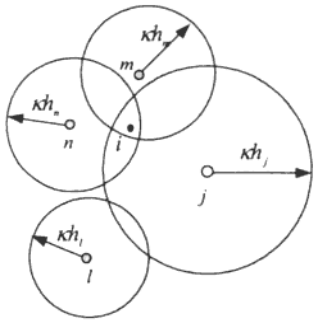

Fig. 1. Scatter model for the concept of influence domain.

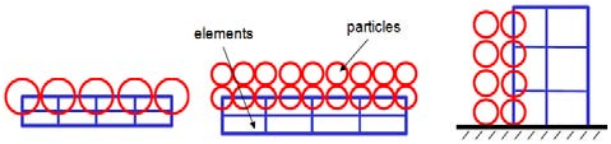

Fig. 2. Contact algorithm between the FEM and SPH: (a) Node to node join; (b) Node to mid-face node join; (c) Arbitrary node to face join.

2.2 Coupled method of FEM and SPH

The SPH method conducts the numerical analysis focusing on the impact of each particle. Accurate analysis depends on the influence domain of the particle and it is defined as the smoothing length, which is the spatial distance between particles. Fig. 1 represents the concept of the influence domain using the smoothing length κh [6]. The analysis to determine the appropriate smoothing length has been carried out and the proper value is selected as 1/5 or 1/10.

In this study, the projectile and bumper plates are modeled using the SPH to simulate the fragment movement, while the final rear plate is modeled based on the FEM to determine whether it is finally penetrated or not. Therefore, an appropriate contact algorithm between the SPH particle and the FE modeled plate is required. Fig. 2 shows various contact algorithm used for the coupling analysis [12]. This study adopts the algorithm of node and mid-face node joining in which double particles are assigned against a single element.

To verify the adopted methods, simulations results are compared with those of previous experimental works as explained in Fig. 3 [19]. Table 2 shows the comparison between experiment and analysis data and the verification is focused on reviewing whether the final rear plate is penetrated or not. In both cases of test 1 and 2, it can be confirmed that the results are well matched.

Table 2. Result comparison of the experiment with the simulation.

Conditions		
Test number	Projectile diameter (mm)	Velocity (km/s)
1	7.9	5.4
2	10	5.71
The result of experiment		
Test 1	Test 2	
Penetration	Penetration	
The result of simulation		
Test 1	Test 2	
Penetration	Penetration	

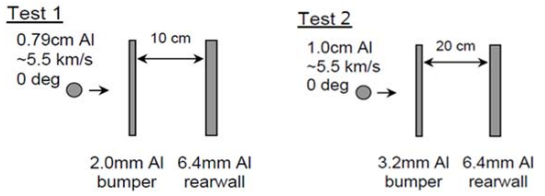

(a) (b)

Fig. 3. Impact test experiment set up: (a) Setting for test 1; (b) Setting for test 2.

2.3 Element erosion scheme

In case of using the FEM for hypervelocity impact analysis, the erosion scheme can be adopted to avoid excessive element deformation causing numerical error [15]. In this study, the final rear plate is represented as the FE modeling and some element may deform beyond the numerical limit especially when the penetration occurs.

The erosion condition is defined according to the incremental geometrical strain defined as follows:

$$\varepsilon_{incr} = \int_0^t \sqrt{\frac{2}{3}\dot{\varepsilon}_{ij}\dot{\varepsilon}_{ij}}\, dt \,. \tag{3}$$

Here, a limit of the incremental geometrical strain is set to 100%, by comparing the experiment results displayed in Table 2.

2.4 Verification of the analysis set up

To verify the analysis setting explained above, the simulation result is compared with the experiment data studied by Piekutowski [17]. The impact experiment is set for the definitive projectile which penetrates a bumper plate and the X-ray photo for the debris distribution is taken for the time period of 6μs. The experiments numbered as 4-1289, 4-1291 and 4-1353 are performed for the conditions displayed in Table 3.

As shown in the above Fig. 4(a), three gauges are positioned to measure the particle velocity after the penetration set in the regular position. Similarly, three gauges are located as displayed in Fig. 4(b) and simulation results by AUTODYN

Table 3. Configuration of three experiments for the comparison (by Piekutowski [17]).

Test no.	Impact velocity (km/s)	Plate thickness (mm)
4-1289	6.68	0.800
4-1291	6.71	1.549
4-1353	6.68	4.039

Table 4. Velocity value comparison at gauges by experiments and SPH simulations.

Axial velocity (km/s)	Gauge 1	Gauge 2	Gauge 3
Experiment 4-1289	6.6	6.4	4.9
SPH (AUTODYN)	6.85	6.45	4.83
Error (%)	3.79	0.78	1.43
Experiment 4-1289	6.3	6.1	3.9
SPH (AUTODYN)	6.44	6.24	3.91
Error (%)	2.22	2.29	0.26
Experiment 4-1289	5.3	5.3	N/A
SPH (AUTODYN)	5.25	5.5	3.35
Error (%)	0.94	3.77	N/A

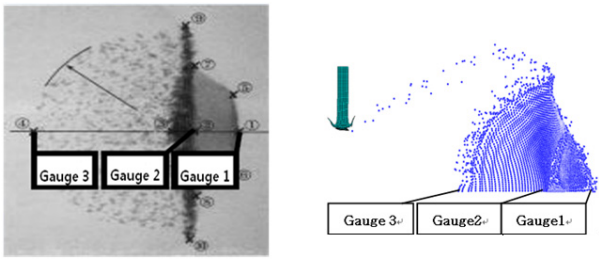

(a) (b)

Fig. 4. Gauge locations for the comparison of experiment and SPH simulation: (a) in the experiment; (b) in the simulation.

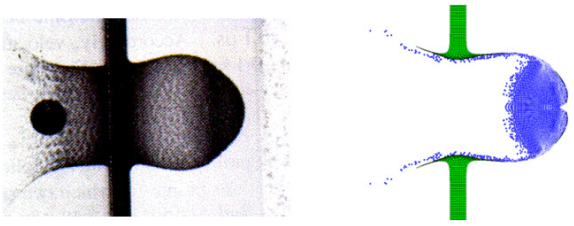

(a) (b)

Fig. 5. Debris clouds at 6μs for test 4-1353: (a) by experiment; (b) by SPH simulation.

are verified by comparison of the velocity values at the gauges. Fig. 5 shows debris cloud distributions by experiment and simulation for test 4-1353 case listed in Table 3.

Velocity values measured at three gauges by experiments and simulations are displayed in Table 4. As shown in the table, simulated data are in 5% error range compared with experimental data and the validity of the SPH simulation can be confirmed.

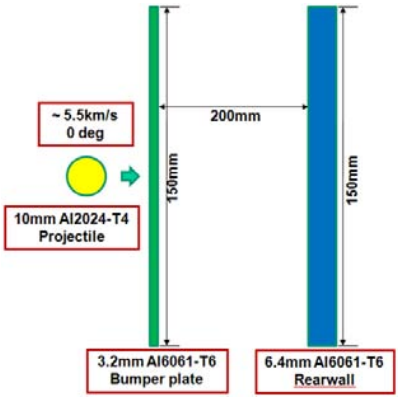

Fig. 6. The first target model for the impact analysis and design.

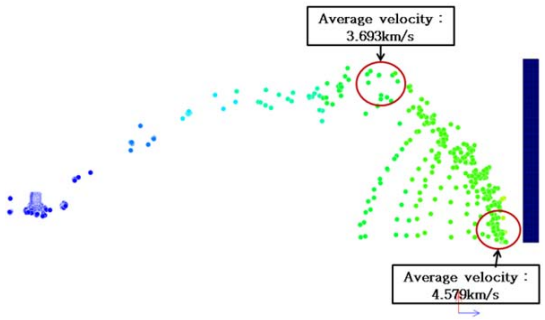

Fig. 7. Average velocity comparison of inside and outside debris.

Fig. 8. Design variable assignment for the first example.

3. Optimization examples

3.1 First example

3.1.1 Design target and modeling

The first target model is selected from the previous work by NASA JSC and Japan (NASDA) as described in Fig. 6 [19]. The model consists of a projectile and two plates. The projectile is made of Al2024-T4 with its diameter of 10 mm. The impact velocity is set to 5.5 km/s with no oblique angle. The thickness of the bumper plate is 3.2 mm with its size of 150×150 mm and Al6061-T6 is used for the material. The last rear plate has the same size and material with the bumper plate with 6.4 mm thickness. For the numerical simulation, only the half model is considered due to the symmetric condition. The projectile and bumper plates are modeled using the SPH, and the rear plate is using the FEM. The projectile and the bumper plates are composed of 372 and 620 particles, respectively, for SPH simulation and the rear plate is modeled by 1170 finite elements.

3.1.2 Design objective and variables

In structural design for the hypervelocity impact case, the basic objective is minimizing total structure weight and maximizing the stiffness to improve the protection effect. The design constraint involves keeping the distance between the bumper plate and the rear plate to avoid the volume expansion. The most important condition in this study is to prevent the rear plate from penetration by debris. Therefore, the optimization problems can be expressed as follows:

$$\begin{aligned} &Minimize\ \ (Plastic\ work\ \&\ Total\ mass\ \ of\ \ the\ structure)\\ &Subject\ to\ \ (Total\ thickness\ constra\,\text{int}\\ &\qquad\ \&\ No\ penetration\ \ of\ \ the\ rear\ \ plate)\,. \end{aligned} \tag{4}$$

Nodes located at the upper end part of each plate are fixed to all degrees of freedom and axial symmetry model is used. The size of the plate is arranged as 75×75 mm. As can be confirmed in Fig. 7, the average velocity of the debris located along the centerline is faster than that of outside debris. Therefore, it is not necessary to make the plate size large, and the analysis time can be reduced by preventing the unnecessary part from modeling. Design variables are set to the bumper plate thickness (t_1) and the rear plate thickness (t_2) as described in Fig. 8, and the rear plate and the distance is fixed as explained above.

3.1.3 Design process and results

The multi-objective optimization [3] is conducted by using the approximate functions of the plastic work and total mass based on the result of the design of experiment (DOE) and the response surface method (RSM). By using the formula (4), the optimization problem can be formulated as

$$\begin{aligned} &Minimize\ \ F(t_1,\ t_2) = w\frac{M}{M_0} + (1-w)\frac{P}{P_0}\\ &Subject\ to\ \ t_1 + t_2 \le 209.6mm\ \ \&\ \ No\ penetration \end{aligned} \tag{5}$$

where M_0 is the initial total mass, P_0 is the initial plastic work and w is the weighting value. As shown in Fig. 8, the thicknesses of the bumper plate and the rear plate are represented as t_1 and t_2, respectively.

The parameter optimization process is conducted based on the initial model using the numerical result. First, the tentative optimal values of design variables are obtained through the DOE process, and based on the values, detailed optimal values are derived through the RSM. In the DOE process, three levels are selected for two design variables as shown in Table 5, and L9 (3^4) orthogonal array is used for numerical experiments as displayed in Table 6. Experiment results are also given in Table 6 with the weighting value of 0.5. Fig. 9 shows the sensitivity graph for each design variable. Optimal levels of the bumper plate thickness (t_1) and the rear plate thickness (t_2) are defined as third and first level, respectively.

Table 5. Design variable levels for the DOE process.

Design variable	Level 1 (mm)	Level 2 (mm)	Level 3 (mm)
t_1	3.0	3.2	3.4
t_2	6.2	6.4	6.6

Table 6. L9 (3^4) orthogonal array for the DOE process.

No.	t_1 level	t_2 level	Plastic work (J)	Total mass (g)	F (w = 0.5)
1	1	1	1007.6	1757.787	1.000
2	1	2	1048.4	1795.999	1.031
3	1	3	1039.2	1834.213	1.037
4	2	2	1006.8	1834.213	1.021
5	2	3	993.55	1872.425	1.026
6	2	1	1023.5	1795.999	1.019
7	3	3	802.89	1910.638	0.948
8	3	1	794.01	1834.213	0.916
9	3	2	781.63	1872.425	0.920

Table 7. Definition of control factor (CF) level for the RSM process.

CF level	-1.414	-1	0	1	1.414
Level 1 (mm)	3.0	3.2	3.4	3.6	3.8
Level 2 (mm)	5.8	6.0	6.2	6.4	6.6

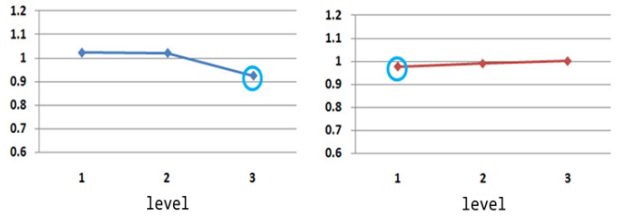

(a) (b)

Fig. 9. Sensitivity graph of design variables for (a) sensitivity level of the bumper plate thickness; (b) sensitivity level of the rear plate thickness.

Tentative optimal values determined through the DOE process are used for the center points for the control factor levels used in the next RSM process as shown in Table 7. The central composite design (CCD) array is set as in Table 8 and numerical results are also displayed in the table. It is noteworthy that the non-penetration condition must be checked because experimental data for penetration cases are not acceptable for the further process.

Using the results of Table 8, regression functions for the plastic work P and total mass M are obtained as the following Eqs. (6) and (7) respectively.

$$P = -1.39582 \times t_1^2 + 1.48755 \times t_2^2 - 4.335 \times t_1 \cdot t_2 - 179.88277 \times t_1 - 1.01749 \times t_2 + 794.01433 \quad (6)$$

Table 8. CCD array for the plastic work and total mass.

No	CF Level 1	CF Level 2	Plastic work (J)	Mass (g)
1	-1	-1	984.4	1757.8
2	1	-1	554.3	1834.2
3	-1	1	1006.8	1834.2
4	1	1	559.3	1910.6
5	0	0	794.0	1834.2
6	0	0	794.0	1834.2
7	1.414	0	610.7	1910.6
8	-1.414	0	1007.6	1757.8
9	0	1.414	802.3	1910.6
10	0	-1.414	827.5	1757.8

Table 9. Comparison of the Pareto optima result of between approximate and analysis value.

	Weight (P:M)	1.0:0.0	0.9:0.1	0.8:0.2
Approximate value	P	529.74	533.99	549.95
	M	2050.28	1926.066	1834.21
Analysis value	P	578.21	608.53	653.02
	M	1987.06	1929.74	1834.21
	Weight (P:M)	0.7:0.3	0.6:0.4	0.5:0.5
Approximate value	P	549.95	549.95	549.95
	M	1834.21	1834.21	1834.21
Analysis value	P	653.02	653.02	653.02
	M	1834.21	1834.21	1834.21
	Weight (P:M)	0.4:0.6	0.3:0.7	0.2:0.8
Approximate value	P	587.91	623.28	1041.32
	M	1813.25	1798.97	1618.15
Analysis value	P	761.71	807.00	1056.60
	M	1815.11	1795.99	1681.36
	Weight (P:M)	0.1:0.9		0.0:1.0
Approximate value	P	1041.32		1041.32
	M	1618.15		1618.15
Analysis value	P	1056.60		1056.60
	M	1681.36		1681.36

$$M = 27.03275 \times t_1^3 + 27.03275 \times t_2^3 + 11.18001 \times t_1^2 \cdot t_2 + 11.18001 \times t_2^2 \cdot t_1 + 1834.21259 \quad (7)$$

The commercial statistic program, SAS 9.2, is used to derive the functions and the R-square values of each function are estimated as 90% and 100%.

Table 9 shows the results comparison of the optimal model according to the various weighting values. The approximate value is calculated using the regression functions of Eqs. (6) and (7), while the analysis value is obtained through the numerical analysis with optimized design variables. If the plastic

Table 10. Result comparison between the initial and the optimal model for the first optimization example.

P:M (0.8:0.2)		Bumper plate (mm)	Rear plate (mm)
Initial model		3.2	6.4
Optimal model	Approximate value	3.8	5.8
	Analysis value		

P:M (w = 0.8)		Plastic Work (J)	Mass (g)	Design objective (F)
Initial model		1006.8	1834.212	1
Optimal model	Approximate value	549.95	1834.212	0.6369
		45.38% ↓	0%	36.31% ↓
	Analysis value	653.02	1834.212	0.7189
		35.14% ↓	0%	28.11% ↓

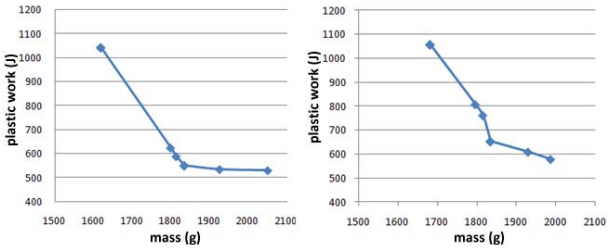

(a) (b)

Fig. 10. Pareto optima graphs based on (a) approximate value; (b) analysis value.

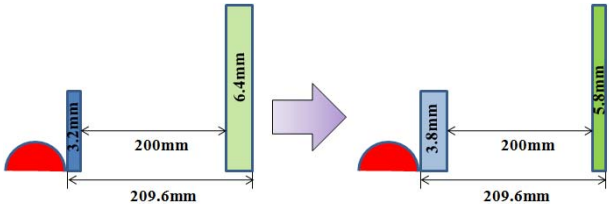

(a) (b)

Fig. 11. Schematic shape comparison: (a) initial model; (b) final optimal model.

work value decreases, the total mass increases. Therefore, results show the traditional Pareto optima patterns as can be confirmed in Fig. 10 both for results based on the approximate function and the numerical analysis.

The case of weighting value of 0.8 is selected as the appropriate results since it can give the minimum plastic work without increasing total mass. Table 10 shows the comparison of the initial and the optimal model. As a result, the thickness of the bumper plate is increased by as much as 0.6 mm and that of the rear plate is decreased by 0.6 mm compared with the initial model. The total plastic work is reduced about 45% and 35% based on the approximate and the analysis values, respectively, while the total mass is maintained. Fig. 11 shows the shape comparison of the initial model with the optimized model.

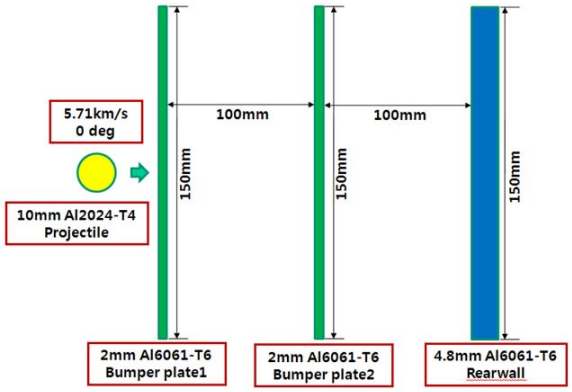

Fig. 12. The second target model for impact analysis and design.

3.2 Second example

3.2.1 Design target and modeling

The second target model is composed of a sphere type projectile, two bumper plates and the rear plate as displayed in Fig. 12. The second initial model is arranged by using the experiment model in NASA JSC and Japan (NASDA) [19]. The projectile is made of Al2024-T4 with 10 mm diameter and the impact velocity of 5.71 km/s. For two bumper plates, Al6061-T6 is selected as the material and their sizes are 150×150 mm with 2 mm thickness. The material of the rear plate is the same as the bumper plate with its thickness of 4.8 mm. Similar to the first optimization case, half model is used for the analysis and design. For the SPH analysis, particle numbers of the projectile, first bumper and the second bumper are 232, 250 and 625, respectively. The rear plate is composed of 564 finite elements.

3.2.2 Design objective and variables

Differently from the first optimization case, the object is only to minimize the total mass and the volume of the system in the second optimization problem. Therefore, the distance between the first bumper plate and the final rear plate can be smaller than the initial value while the non-penetration constraint for the final rear plate must be kept. There are five design variables, which are three thicknesses of two bumper plates and the rear plate and two distances between each of plates as can be displayed in Fig. 13. Therefore, the optimization problem can be formulated as follows:

$$\begin{aligned} &Minimize\ F(t_1,\ t_2,\ t_3,\ t_4,\ t_5) = w\frac{M}{M_0} + (1-w)\frac{V}{V_0} \\ &Subject\ to\ \ t_1 + t_2 + t_3 + t_4 + t_5 \le 208.8mm\ \ \&\ \ No\ penetration \end{aligned} \tag{8}$$

where M_0 is the initial total mass, V_0 is the initial total volume and w is the weighting value. Because the Pareto optima relation does not occur in this case, the weighting value is set to

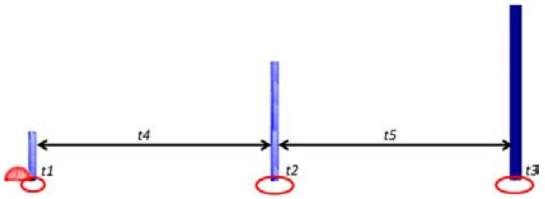

Fig. 13. Design variable assignment for the second example.

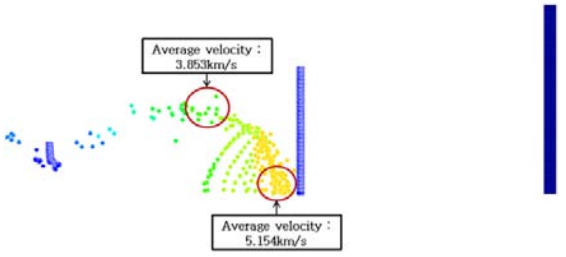

(a)

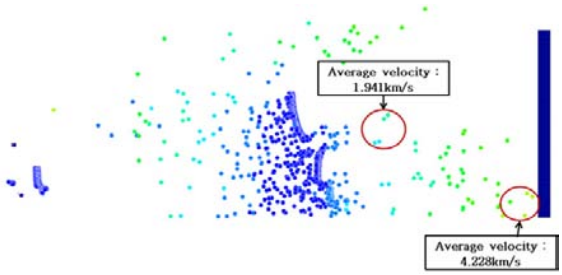

(b)

Fig. 14. Average velocity comparison of inside and outside debris: (a) before hitting the second bumper plate; (b) before hitting the rear plate.

0.5. As boundary conditions, the upper end part of each plate is constrained to all degrees of freedom. As can be confirmed in Fig. 14, the debris velocity along the symmetric centerline is much faster than that of the outside debris. Therefore, the plate size can be reduced to minimize the analysis time. In this study, sizes of the first bumper plate, the second bumper plate and the final rear plate are set to 20×20 mm, 60×60 mm and 75×75 mm.

3.2.3 Design process and results

Among the five design variables, sensitive design variables are verified by using the DOE process. The L18 ($2^1 \times 3^7$) orthogonal array is adopted for numerical experiments using three levels as shown in Table 11 and results are given in Table 12. Fig. 15 shows the sensitivity graphs for each design variable, and it can be confirmed that the rear plate thickness (t_3) and two distance variables (t_4 and t_5) are the most sensitive variables. The optimal levels are determined as 3.6 mm, 75 mm and 75 mm for t_3, t_4 and t_5, respectively. Those values are used as the center values during the next RSM process. Thicknesses of the two bumper plates are set to 2 mm finally.

The RSM process is succeeded to determine the optimal values of the selected three design variables and their levels

Table 11. Design variable levels for the DOE process.

Design variables	Level 1 (mm)	Level 2 (mm)	Level 3 (mm)
t_1	1.5	2	3
t_2	1.5	2	3
t_3	3.6	4.8	6
t_4	75	100	125
t_5	75	100	125

Table 12. L18 ($2^1 \times 3^7$) orthogonal array for the DOE process.

Run	Levels					Total mass (g)	Volume (mm^3)	F (w = 0.5)
	t_1	t_2	t_3	t_4	t_5			
1	1	1	1	1	1	315.2553	2767350	0.7500
2	1	2	2	2	2	396.4574	3680965	0.9704
3	1	3	3	3	3	501.5425	4603415	1.2204
4	2	1	1	2	2	339.1383	3659759	0.8993
5	2	2	2	3	3	420.3404	4573374	1.1197
6	2	3	3	1	1	525.4255	2845105	1.0105
7	3	1	2	1	3	444.2234	3698636	1.0296
8	3	2	3	2	1	525.4255	3286891	1.0704
9	3	3	1	3	2	458.5531	4145724	1.1072
10	1	1	3	3	2	429.8936	4135121	1.0717
11	1	2	1	1	3	339.1383	3659759	0.8993
12	1	3	2	2	1	444.2234	3256850	0.9697
13	2	1	2	3	1	396.4574	3680965	0.9704
14	2	2	3	1	2	477.6595	3269220	1.0112
15	2	3	1	2	3	410.7872	4128053	1.0480
16	3	1	3	2	3	501.5425	4161629	1.1605
17	3	2	1	3	1	410.7872	3686266	0.9882
18	3	3	2	1	2	515.8723	3283357	1.0586

are selected as displayed in Table 13. The central composite design (CCD) array is defined as in Table 14 with numerical results. The natural variable values are converted into the coded variable values for the numerical simulation by AUTODYN. Similar to the first optimization case, if the numerical simulation result using the selected level gives the penetration of the final rear plate, the result is not included to derive the regression functions because it violates the non-penetration constraint.

Based on the results in Table 14, the regression functions for the total mass and the volume are determined as follows:

$$\begin{aligned} M =& 0.04477 \times t_3^2 - 0.00694 \times t_4^2 - 0.00694 \times t_5^2 \\ &+ 0.80512 \times t_4 \cdot t_5 + 5.96384 \times t_3 + 363.02131 , \end{aligned} \tag{9}$$

$$\begin{aligned} V =& -885.709 \times t_1^2 + 1390.8147 \times t_2^2 + 3523.5057 \times t_3^2 \\ &+ 20685 \times t_1 \cdot t_2 + 297.8609 \times t_2 \cdot t_3 + 14893 \times t_1 \cdot t_3 \\ &+ 2206.3786 \times t_1 + 110319 \times t_2 + 153221 \times t_3 + 2785031 . \end{aligned} \tag{10}$$

Table 13. Definition of the control factor level for the RSM process.

Level (mm)	-1.73	-1	0	1	1.73
CF1 (t_3)	3.387	3.492	3.6	3.708	3.819
CF2 (t_4)	64.589	69.6	75	80.4	86.189
CF3 (t_5)	60.75	67.5	75	82.5	90.75

Table 14. CCD array for the total mass and the volume.

Run	t_3 (mm)	t_4 (mm)	t_5 (mm)	Mass (g)	Volume (mm^3)
1	3.708	80.4	67.5	368.1799	2749820.3
2	3.708	69.6	82.5	368.1799	2824040.5
3	3.492	80.4	82.5	357.8625	3011075.2
4	3.492	69.6	67.5	357.8625	2555151.6
5	3.387	75	75	352.8586	2781262.1
6	3.819	75	75	373.4934	2788896.2
7	3.6	64.589	75	363.0212	2601040.8
8	3.6	86.189	75	363.0212	2982744.3
9	3.6	75	60.75	363.0212	2533203.6
10	3.6	75	90.75	363.0212	3063347.4
11	3.6	75	75	363.0212	2785021.9
12	3.6	75	75	363.0212	2785021.9
13	3.6	75	75	363.0212	2785021.9
14	3.6	75	75	363.0212	2785021.9

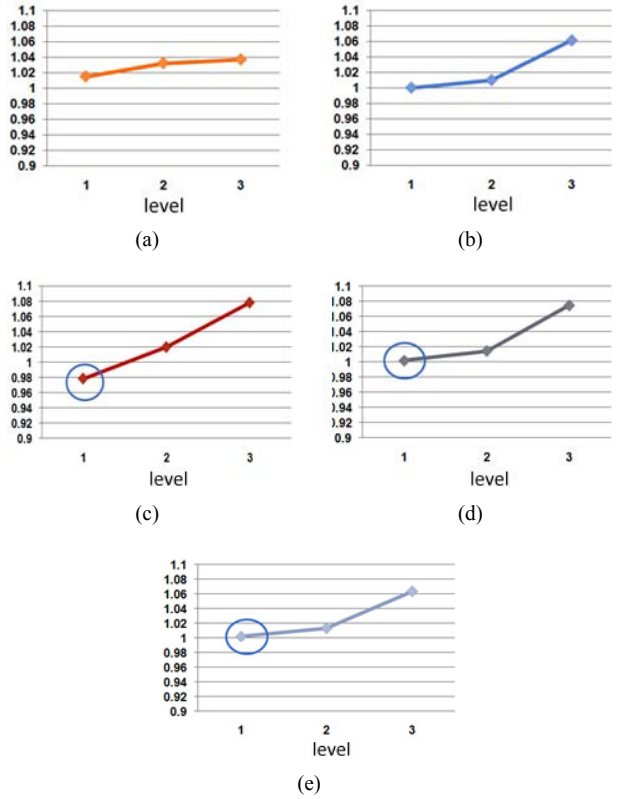

Fig. 15. Sensitivity graph of design variables: (a) sensitivity level of the first bumper plate; (b) sensitivity level of the second bumper plate; (c) sensitivity level of the rear plate; (d) sensitivity level of the distance between two bumper plates; (e) sensitivity level of the distance between the second bumper plate and the rear plate.

Table 15. Optimization result comparison between the initial and the optimal model for the second optimization case.

P:M (0.5:0.5)		1st Bumper plate (mm)	2nd Bumper plate (mm)	Rear plate (mm)
Initial model		2	2	4.8
Optimal model	Approximate value	2	2	3.82
	Analysis value			

P:M (0.5:0.5)		1st Distance (mm)	2nd Distance (mm)
Initial model		100	100
Optimal model	Approximate value	64.59	60.75
	Analysis value		

P:M (0.5:0.5)		Mass (g)	Volume (mm^3)	Design objective
Initial model		420.35	3689800.57	1
Optimal model	Approximate value	375.84	2239391.10	0.7505
		10.59%↓	39.31%↓	24.95%↓
	Analysis value	373.49	2353096.80	0.7631
		11.15%↓	36.23%↓	23.69%↓

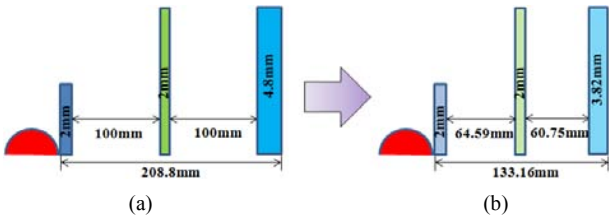

Fig. 16. Schematic shape comparison for second optimization: (a) initial model; (b) final optimal model.

According to SAS 9.2 verification, the R-square values of each regression functions are scored 100% and 99%, respectively.

As a result, the thickness of the rear plate is decreased as 0.78 mm and the distance between the two plates and that between the second bumper plate and the rear plate is reduced as much as 35.41 mm and 39.25 mm, respectively. The total mass is reduced by about 10.6% and 11.1% based on the approximate and the analysis values, respectively, while the volume is decreased about 39.3% and 36.2% according to the approximate and the analysis values, respectively. Table 15 shows the comparison of the initial and the optimal mode, and Fig. 16 shows the shape comparison of the initial model with the optimal model.

4. Conclusions

The impact simulation and optimization process is conducted for the purpose of minimizing the satellite structure damage caused by hypervelocity debris impact. The combined SPH and the FEM methodology is used to simulate the debris

effect. The analysis has been performed using the commercial package AUTODYN. Various pre-conditions for accurate analysis have been determined by comparison of simulation results with previously published experimental results.

The optimization process composed of the DOE and the RSM has been performed. The DOE is adopted to determine the sensitive design variables and their preliminary optimal levels, while the RSM is used to obtain the final detail optimal result. The first optimization problem is targeted to minimize the plastic energy as well as the total weight to reduce the damage effect on the final rear plate and the structure is composed of a bumper plate and a rear plate. On the contrary, the second optimization problem is focused on minimizing the mass and the volume of the system. Another bumper plate is added so that various effects caused by several design variables can be considered. As a result, it can be confirmed that the total mass of the structure can be reduced in both problems without violating the constraint of non-penetration of the final rear plate.

Acknowledgment

This work was supported by Defense Acquisition Program Administration and Agency for Defense Development (UD090090AD).

References

[1] S. Ryan, F. Schaefer, R. Destefanis and M. Lambert, A ballistic limit equation for hypervelocity impacts on composite honeycomb sandwich panel satellite structures, *Advances in Space Research*, 41 (2008) 1152-1166.

[2] Y. H. Yoo, S. N. Chang and D. T. Chung, Numerical simulation of high velocity oblique impact of mild steel spheres against mild steel plates, *Transactions of the KSME A*, 26 (3) (2002) 576-585.

[3] M. S. Park, J. H. Yoo and D. T. Chung, An optimization of a multi-layered plate under ballistic impact, *International Journal of Solids and Structures*, 42 (1) (2005) 123-137.

[4] M. S. Park, J. H. Yoo and D. T. Chung, Numerical and experimental approach of a dual plate under ballistic impact for an optimal design, *International Journal of Modern Physics* 22 (9-11) (2008) 1538-1543.

[5] J. A. Zukas, *High velocity impact dynamics*, Wiley, New York (1990).

[6] G. R. Liu, M. B. Liu, Smoothed particle hydrodynamics (2003).

[7] K. Shintate and H. Sekine, Numerical simulation of hypervelocity impacts of a projectile on laminated composite plate targets by means of improved SPH method, *Composites*, 35 (2004) 683-692.

[8] O. K. Min, J. H. Lee, K. W. Kim and H. Park, An application of smoothed particle hydrodynamics in analysis of dynamic elasto-plastic deformation, *Proceedings of 2nd ISIE '96* (1996) 392-397.

[9] J. Lopez-Puente, A. Arias, R. Zaera and C. Navarro, The effect of the thickness of the adhesive layer on the ballistic limit of ceramic/metal armours. An experimental and numerical study, *International Journal of Impact Engineering*, 32 (2005) 321-336.

[10] S. S. Lee, S. W. Seo and O. K. Min, SPH parameters for analysis of penetration phenomenon at hypervelocity impact of meteorite, *Transactions of the KSME A*, 27 (10) (2003) 1738-1747.

[11] P. H. L. Groenenboom, Numerical simulation of 2D and 3D hypervelocity impact using the SPH option in PAM-shock, *International Journal of Impact Engineering*, 20 (1997) 309-323.

[12] R. A. Clegg, C. J. Hayhurst and O. F. J. Meuric, Combined mesh and meshfree numerical techniques to efficiently predict the response of concrete structures to impact, *Proceedings of Structures under Shock & Impact* (2000) TP069.

[13] M. H. Lee and S. W. Kim, Development of 2-Dim Lagrangian hydrocode and application to large deformation problems, *Transactions of the KSME A*, 27 (3) (2003) 409-415.

[14] D. W. Park, D. T. Chung and S. I. Oh, Improved contact algorithm for explicit FEM, *Transactions of the KSME A*, 2 (1) (1996) 379-384.

[15] Swedish Defence Research Agency, *A note on an erosion criterion in AUTODYN*, Methodology Report (2002).

[16] ANSYS. Inc., Theory manual of ANSYS AUTODYN (2005).

[17] A. J. Piekutowski, Characteristics of debris clouds produced by hypervelocity impact of aluminum spheres with thin aluminum plates, *International Journal of Impact Engineering*, 14 (1993) 573-586.

[18] C. J. Hayhurst and R. A. Clegg, Cylindrically symmetric SPH simulations of hypervelocity impacts on thin plates, *International Journal of Impact Engineering*, 20 (1996) 337-348.

[19] The Inter-Agency Space Debris Coordination Committee WG3 members, *Protection Manual Version 3.3* (2004).

Younghoon Kim received his B.S. degrees in Aerospace and Mechanical Engineering from Korea Aerospace University, Korea, in 2009. During his studying for Master's degree at Yonsei University, Mr. Kim has studied hypervelocity impact analysis. He is working at Samsung Techwin at the present.